Published in "ACS Applied Materials & Interfaces 12(16): 18496–18503, 2020"
which should be cited to refer to this work.

$Li_{0.5}Ni_{0.5}Ti_{1.5}Fe_{0.5}(PO_4)_3$/C Electrode Material for Lithium Ion Batteries Exhibiting Faster Kinetics and Enhanced Stability

Mohammed Srout, Nam Hee Kwon, Hicham Ben Youcef, Nawal Semlal, Katharina M. Fromm, and Ismael Saadoune*

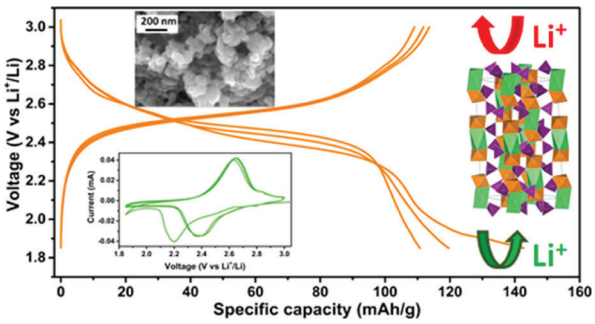

ABSTRACT: Natrium super ionic conductor (NASICON) materials providing attractive properties such as high ionic conductivity and good structural stability are considered as very promising materials for use as electrodes for lithium- and sodium-ion batteries. Herein, a new high-performance electrode material, $Li_{0.5}Ni_{0.5}Ti_{1.5}Fe_{0.5}(PO_4)_3$/C, was synthesized via the sol−gel method and was electrochemically tested as an anode for lithium ion batteries, providing enhanced electrochemical performance as a result of nickel substitution into the lithium site in the $LiTi_2(PO_4)_3$ family of materials. The synthesized material showed good ionic conductivity, excellent structural stability, stable long-term cycling performance, and improved high rate cycling performance compared to $LiTi_2(PO_4)_3$. The $Li_{0.5}Ni_{0.5}Ti_{1.5}Fe_{0.5}(PO_4)_3$/C electrode delivered reversible capacities of about 93 and 68% of its theoretical one at current rates of 0.1 C (6.42 mA·g^{-1}) after 100 cycles and 5 C (320.93 mA·g^{-1}) after 1000 cycles, respectively. Theoretically, three Li^+ ions can be inserted into the vacancies of the $Li_{0.5}Ni_{0.5}Ti_{1.5}Fe_{0.5}(PO_4)_3$/C structure. However, when the electrode is discharged to 0.5 V, more than three Li^+ ions are inserted into the NASICON structure, leading to its structural transformation, and thus to an irreversible electrochemical behavior after the first discharge process.

KEYWORDS: *phosphate, NASICON, fast kinetics, high rate capability, lithium-ion batteries*

■ INTRODUCTION

In order to face the growing demands in energy and to limit the growing environmental pollution and global warming, the use of eco-friendly and renewable energy sources as alternatives to the widely used fossil resources has attracted much interest worldwide.[1,2] In particular, highly effective energy storage devices are required as complementary systems toward the use and development of these new energy sources. Li-ion batteries (LIBs), exhibiting great potential because of their high volume and gravimetric energy density, stand as the convenient candidates.[1,3−5]

Among the various existing electrode materials, including oxides, and carbonaceous and polyanionic materials, phosphate-based natrium super ionic conductor (NASICON) structure-type compounds exhibiting high structural and thermal stabilities, in addition to their fast ionic conductivity, are attractive materials for use in energy storage devices, namely LIBs and sodium-ion batteries (SIBs).[6,7] They have been tested as both cathode and anode materials[6,8,9] thanks to their very rich and various compositions. NASICON materials generally exist with the general formula $A_xM_2(PO_4)_3$, where "A" can be either monovalent (Li^+ or Na^+) or divalent (Ni^{2+}, Mg^{2+}, Ca^{2+}, Mn^{2+}, etc.) ions and M is a transitional metal (Ti, Fe, V, Zr, Sc, etc.).[10] Among these materials, $A_xTi_2(PO_4)_3$ is usually considered as a negative electrode because of its low working voltage versus Li^+/Li (∼2.5 V).[11,12] However, similar to other phosphate-based materials such as olivine cathodes,[13] the use of the NASICON-type phosphates is limited because of the low electronic conductivity resulting from the long M−M distance (existence of −M−O−P−O−M− linking) in their structural framework. To overcome this inconvenience, carbon coating and chemical substitution (or doping) are considered as efficient methods in order to improve the electrochemical performance of these materials, mainly their rate capability.[11,13,14]

Aiming to enhance the structural stability and electrochemical properties of the previously studied $Li_{1.5}Ti_{1.5}Fe_{0.5}(PO_4)_3$ NASICON-type material,[14] a novel substitution strategy targeting the A (Li) site is considered. Among several transition metals, nickel was used as a substitute because of its attractive properties, mainly the ionic radius of

Ni^{2+} ions (R_{Ni}^{2+} = 0.69 Å) which can be considered to be of the same order as that of lithium (R_{Li}^{1+} = 0.74 Å). This property would ensure an optimized interstitial channel size for lithium diffusion in the structure during the intercalation/de-intercalation processes.[15,16]

In this work, the $Li_{0.5}Ni_{0.5}Ti_{1.5}Fe_{0.5}(PO_4)_3$ material was synthetized via the sol−gel method and its particles were carbon-coated using sucrose as the carbon source. X-ray diffraction (XRD) allowed us to confirm the NASICON structure of the obtained composite material, using the Rietveld method to refine the lattice parameters, the atomic positions, and the inner-atomic distances. Scanning electron microscopy (SEM) and transmission electron microscopy (TEM) allowed us to analyze the morphology of the pristine and composite materials. Raman spectroscopy was used to monitor the carbon coating of the composite material and to confirm its NASICON structure. The electrochemical performance of $Li_{0.5}Ni_{0.5}Ti_{1.5}Fe_{0.5}(PO_4)_3$/C was tested via galvanostatic test methods and cyclic voltammetry (CV). The impedance of the $Li_{0.5}Ni_{0.5}Ti_{1.5}Fe_{0.5}(PO_4)_3$/C electrode-based cell was studied during the first discharge−charge process using electrochemical impedance spectroscopy (EIS). Lithium diffusion kinetics during the first discharge process were also studied using the galvanostatic intermittent titration technique (GITT) and CV at different scan rates.

EXPERIMENTAL METHODS

Synthesis. $Li_{0.5}Ni_{0.5}Ti_{1.5}Fe_{0.5}(PO_4)_3$ was synthesized via a conventional sol−gel method, as described in our previous work.[14] First, stoichiometric amounts of anhydrous $Li(OOCCH_3)$ (99.998%; Aesar PURATRONIC) (2.51 mmol), $Ni(OOCCH_3)_2{\cdot}4H_2O$ (99.0%; Sigma-Aldrich) (2.4 mmol), and $Fe(NO_3)_3{\cdot}9H_2O$ (98.0%; Sigma-Aldrich) (2.4 mmol) were dissolved in about 15 mL of ethanol with stirring for 1 h. Then, H_3PO_4 (85%; Sigma-Aldrich) (14.86 mmol) and $TiCl_4$ (99%; Aldrich) diluted in ethanol (7.19 mmol equivalent of TiO_2) were added into the first solution under continuous stirring. Few drops (about 40−60 μL) of deionized water were added into the mixture to adjust the pH to ∼0 and form a gel. The obtained gel was dried at 100 °C overnight and ball-milled for 30 min at 400 rpm using a planetary ball mill (Retsch PM100) and about 10 balls with different diameters varying between 5 and 15 mm. The obtained powder is then heated to 400 °C for 3 h with a heating rate of 5 °C/min under air, ball-milled again under the same conditions, and then heated up and kept at 700 °C for 12 h under an air atmosphere. Afterward, the resulting powder (85 wt %) was ground with 15 wt % sucrose in acetone (5 mL) for about 10 min using an agate mortar, dried, and annealed at 600 °C for 6 h under an argon flow. The final obtained carbon-coated $Li_{0.5}Ni_{0.5}Ti_{1.5}Fe_{0.5}(PO_4)_3$/C composite was black.

Characterization of the Material. The XRD pattern of the $Li_{0.5}Ni_{0.5}Ti_{1.5}Fe_{0.5}(PO_4)_3$ sample was obtained using a Rigaku Ultima IV diffractometer with Cu Kα radiation (λ = 1.5406 Å), between 2θ = 10 and 60°, with a step of 0.01°. The Rietveld refinement method[17] was used to calculate the structural parameters through the FULLPROF program.[18] A pseudo-Voigt profile function was used to describe the shape of the diffraction lines.

SEM images were captured with a Tescan Mira3 LM FE electron microscope (0.5−30 kV). TEM images were obtained with a Tecnai Spirit instrument (120 kV).

Raman spectra were collected using a Cofotec MR520 3D Raman confocal microscope with a 532 nm beam under ambient conditions.

The carbon content in the composite material was determined by thermogravimetric analysis (TGA), with a heating rate of 10 °C min^{-1} using a Discovery TGA instrument under an air atmosphere.

The specific surface area was calculated at 77 K using the Brunauer−Emmett−Teller (BET) method on a Gemini VII 2390 surface area analyzer (Micromeritics Instrument Corp.). The degassing conditions were set to be 200 °C for 24 h under vacuum for all samples.

Electrochemical Measurements. The electrochemical performances of the $Li_{0.5}Ni_{0.5}Ti_{1.5}Fe_{0.5}(PO_4)_3$/C electrode material were tested in C2030 coin cells, using a mixture of $Li_{0.5}Ni_{0.5}Ti_{1.5}Fe_{0.5}(PO_4)_3$/C, carbon black (Super P), and carboxymethyl cellulose as a binder with a weight ratio of 75:15:10 as the cathode and metallic lithium foil as the anode (counter electrode). The average active material mass loading of the electrodes was about 1.5 mg cm^{-2}. The current and specific capacity are calculated according to the mass of the active material (75%) per electrode. A Celgard membrane was used as a separator, and commercial $LiPF_6$ (1 M) dissolved in 50:50 (by volume) ethylene carbonate/dimethyl carbonate (DMC) was used as the electrolyte. All the electrochemical tests were measured on Biologic MPG2 and SP300 instruments at room temperature (∼25 °C). Lithium diffusion kinetics during the first discharge process were also studied using the GITT and CV with various sweep rates from 0.02 to 0.2 mV s^{-1}. EIS was performed on a Biologic instrument, SP150.

RESULTS AND DISCUSSION

Structure and Morphology. The crystal structure of the synthesized $Li_{0.5}Ni_{0.5}Ti_{1.5}Fe_{0.5}(PO_4)_3$ material was studied by powder XRD. As shown in Figure 1, all the diffraction peaks

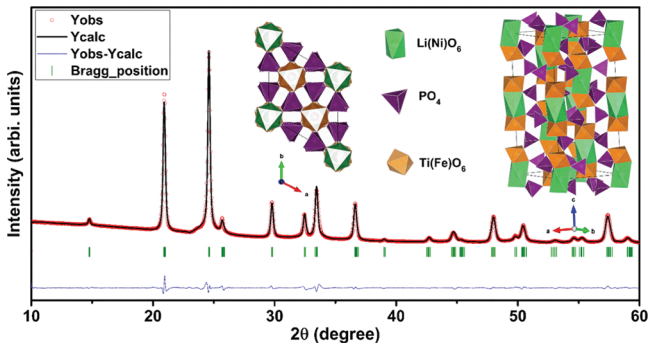

Figure 1. Rietveld refinement of the synthesized $Li_{0.5}Ni_{0.5}Ti_{1.5}Fe_{0.5}(PO_4)_3$ structure based on the powder XRD data and its schematic structure.

can be indexed assuming a rhombohedral symmetry and $R\bar{3}c$ space group implying the high purity of our $Li_{0.5}Ni_{0.5}Ti_{1.5}Fe_{0.5}(PO_4)_3$ material. Rietveld refinement allowed calculating the $Li_{0.5}Ni_{0.5}Ti_{1.5}Fe_{0.5}(PO_4)_3$ related lattice parameters $a(b)$ = 8.4987(3) Å and c = 20.6999(1) Å and cell volume V = 1294 ± 1 $Å^3$. The small values of R_{wp} = 7.44% and R_p = 7.62% (<10%) suggest reasonable refinement results. The $Li_{0.5}Ni_{0.5}Ti_{1.5}Fe_{0.5}(PO_4)_3$ NASICON-type material is constructed with lanternlike units sequenced along the c-axis, where each unit is composed of octahedral $[Ti(Fe)O_6]$ sharing corners (O atoms) with tetrahedral $[PO_4]$, as displayed in the inset of Figure 1.

In this rhombohedral structure, both Ni and Li are supposed to be placed in the more-stable M1 sites, which are located at the Wyckoff position 6b with the site symmetry $\bar{3}$.[19] Accordingly, Table S1 gives more detailed information regarding the atomic position of the different elements constituting the $Li_{0.5}Ni_{0.5}Ti_{1.5}Fe_{0.5}(PO_4)_3$ material, and Table S2 gives the different interatomic distances that were calculated and the average (M-O) bond lengths. The obtained results are in very good agreement with the ones reported for the $LiTi_2(PO_4)_3$ (LTP) material, with a Li−O distance equal to 2.26 Å and Ti−O average distance of 1.9 Å.[19] In addition, the

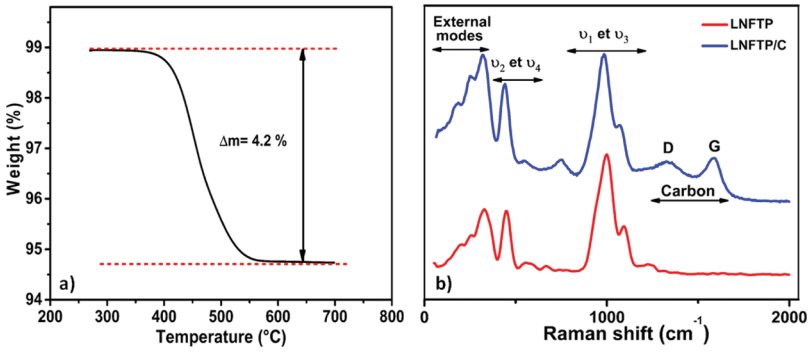

Figure 2. (a) TGA curve of $Li_{0.5}Ni_{0.5}Ti_{1.5}Fe_{0.5}(PO_4)_3/C$ recorded under air with a heating rate of 10 °C min^{-1} and (b) Raman spectra for bare $Li_{0.5}Ni_{0.5}Ti_{1.5}Fe_{0.5}(PO_4)_3$ and the carbon-coated $Li_{0.5}Ni_{0.5}Ti_{1.5}Fe_{0.5}(PO_4)_3/C$.

calculated cell volume was in good agreement with the one obtained for the LTP material.[19,20] These results confirmed our first hypothesis of putting Li and Ni of the $Li_{0.5}Ni_{0.5}Ti_{1.5}Fe_{0.5}(PO_4)_3$ material at the same more-stable M1 site, similar to Li in LTP. Furthermore, the XRD pattern of the $Li_{0.5}Ni_{0.5}Ti_{1.5}Fe_{0.5}(PO_4)_3/C$ composite was also obtained and no changes of the crystal structure were observed after the carbon-coating process (Figure S1).

Raman spectroscopy (Figure 2b) was also employed for both pristine $Li_{0.5}Ni_{0.5}Ti_{1.5}Fe_{0.5}(PO_4)_3$ powder and the $Li_{0.5}Ni_{0.5}Ti_{1.5}Fe_{0.5}(PO_4)_3/C$ composite material in order to confirm the NASICON structure and the presence of the carbon coating on the composite material.[14]

Raman spectra of $Li_{0.5}Ni_{0.5}Ti_{1.5}Fe_{0.5}(PO_4)_3/C$ show the appearance of two extra bands at 1326 and 1590 cm^{-1}, attributed to the D and G bands and characteristic of the carbon coating. The intensity ratio of I_D/I_G is 0.96, which is a sign of a highly disordered carbon structure.[21−23] TGA measurement gave the carbon amount in the $Li_{0.5}Ni_{0.5}Ti_{1.5}Fe_{0.5}(PO_4)_3/C$ composite material, which was determined to be ∼4.2 wt % (Figure 2a). The BET specific surface areas of the $Li_{0.5}Ni_{0.5}Ti_{1.5}Fe_{0.5}(PO_4)_3$ and $Li_{0.5}Ni_{0.5}Ti_{1.5}Fe_{0.5}(PO_4)_3/C$ are 19.53 and 38.02 m^2 g^{-1}, respectively. The increased surface area of the $Li_{0.5}Ni_{0.5}Ti_{1.5}Fe_{0.5}(PO_4)_3/C$ material is likely due to the formation of porous carbon on the surface of the pristine material.[24]

The morphologies of the $Li_{0.5}Ni_{0.5}Ti_{1.5}Fe_{0.5}(PO_4)_3$ and $Li_{0.5}Ni_{0.5}Ti_{1.5}Fe_{0.5}(PO_4)_3/C$ materials were investigated by SEM and TEM, as shown in Figure 3. The SEM images show that $Li_{0.5}Ni_{0.5}Ti_{1.5}Fe_{0.5}(PO_4)_3/C$ is composed of irregularly shaped and aggregated particles (Figure 3a,b). The morphology of the primary particles can be considered spherical-like with an average diameter of about 60 nm (Figure S2). The corresponding TEM image (Figure 3c) shows the $Li_{0.5}Ni_{0.5}Ti_{1.5}Fe_{0.5}(PO_4)_3$ particles before carbon coating, confirming the morphology and particle size determined via SEM, while the other TEM image (Figure 3d) shows the agglomerated $Li_{0.5}Ni_{0.5}Ti_{1.5}Fe_{0.5}(PO_4)_3$ nanoparticles with a heterogeneous thin layer of carbon coating on the surface of some particles.

Electrochemistry. *Electrochemical Performance.* The electrochemical behavior of the $Li_{0.5}Ni_{0.5}Ti_{1.5}Fe_{0.5}(PO_4)_3/C$ composite material as an electrode for LIBs was investigated in detail using an electrochemical half-cell system within the voltage ranges of 1.85−3.0 and 0.5−3.0 V versus Li^+/Li.

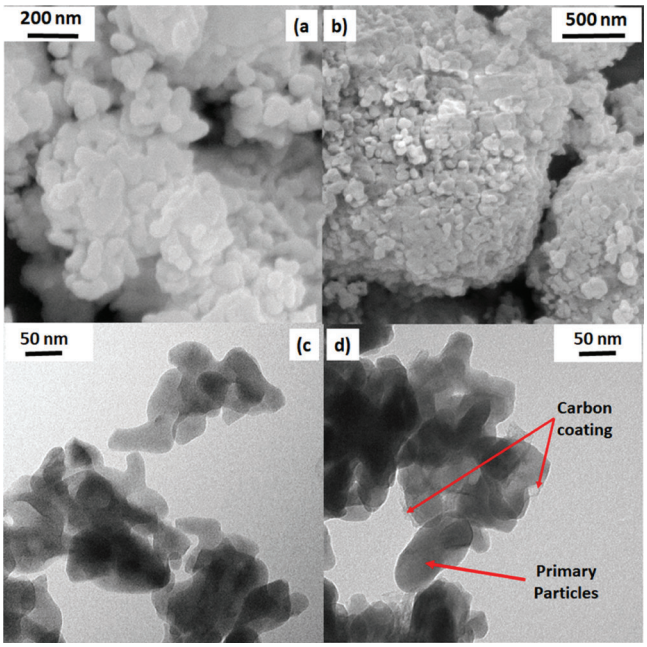

Figure 3. (a,b) SEM images of carbon-coated $Li_{0.5}Ni_{0.5}Ti_{1.5}Fe_{0.5}(PO_4)_3/C$ particles and (c,d) TEM images of bare $Li_{0.5}Ni_{0.5}Ti_{1.5}Fe_{0.5}(PO_4)_3$particles (c) and the carbon-coated $Li_{0.5}Ni_{0.5}Ti_{1.5}Fe_{0.5}(PO_4)_3/C$ particles (d).

Figure 4a shows the charge−discharge curves of the $Li_{0.5}Ni_{0.5}Ti_{1.5}Fe_{0.5}(PO_4)_3/C$ material within the voltage window 1.85−3.0 V at 0.1 C current rate. One feature appearing at about 2.8 V can be related to the Fe^{2+}/Fe^{3+} redox couple, while a more important plateau appears at about 2.48 V, which is associated to the Ti^{3+}/Ti^{4+} redox couple.[25]

Theoretically, the reduction of 0.5 Fe^{3+} to Fe^{2+} and 1.5 Ti^{4+} to Ti^{3+} allows the insertion of two lithium ions into the structure, giving a theoretical capacity of about 128 mA h·g^{-1}.

$$Li_{0.5}Ni_{0.5}Ti^{IV}_{1.5}Fe^{III}_{0.5}(PO_4)_3 + 2Li^+ + 2e^- \rightarrow Li_{2.5}Ni_{0.5}Ti^{III}_{1.5}Fe^{II}_{0.5}(PO_4)_3$$

The observed experimental capacity of the first discharge is 142 mA h·g^{-1}; however, this capacity drops to about 120 mA h·g^{-1} afterward. The extra obtained capacity at the first discharge compared to the theoretical one can be related to the solid electrolyte interface (SEI) formation and its participation in the consumption of lithium ions even though the cut-off voltage is higher than 1 V versus Li^+/Li. One can notice that

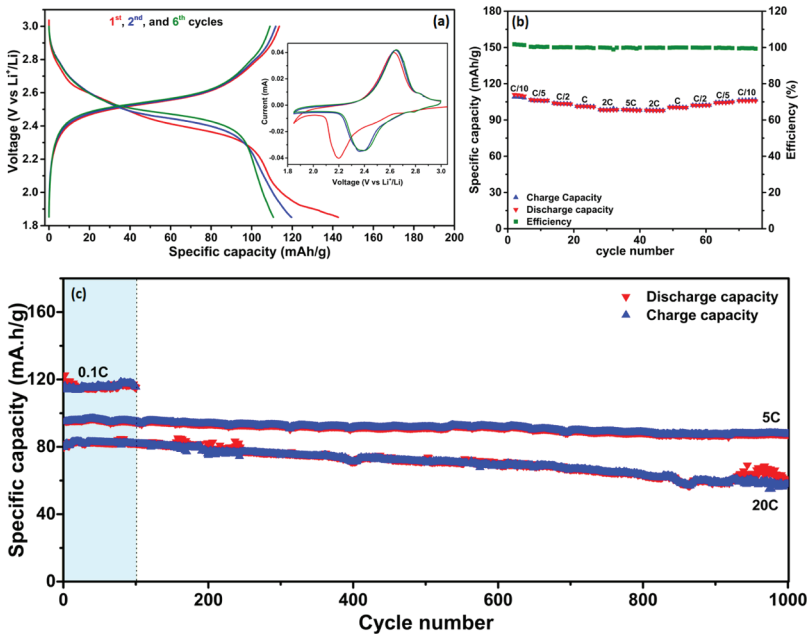

Figure 4. Electrochemical properties of the $Li_{0.5}Ni_{0.5}Ti_{1.5}Fe_{0.5}(PO_4)_3$/C electrode material in the voltage window 1.85−3.0 V vs Li^+/Li: (a) initial charge/discharge profiles at a current rate of 0.1 C—the corresponding CV curves at the slow scan rate of 0.02 mV s^{-1}; (b) rate capability performance (0.1−5 C); (c) long-term cycling at current rates of 0.1 C (100 cycles) and 5 and 20 C (1000 cycles).

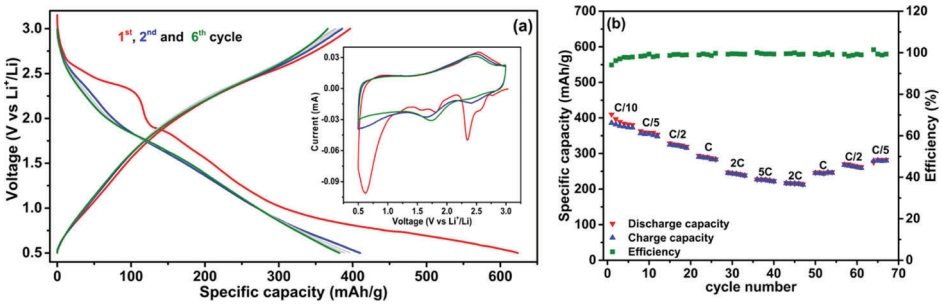

Figure 5. Electrochemical properties of the $Li_{0.5}Ni_{0.5}Ti_{1.5}Fe_{0.5}(PO_4)_3$/C electrode material in the voltage range 0.5−3.0 V vs Li^+/Li: (a) initial charge/discharge profiles at the rate of 0.1 C—the corresponding CV curves at the slow scan rate of 0.02 mV s^{-1} and (b) rate capability performance (0.1−5 C).

the slope seen at the end of the first discharge, which is responsible for the extra capacity, disappears after the first cycle. CV results in the voltage window 1.0−3.0 V versus Li^+/Li (Figure S3) confirm the occurrence of side reactions of the electrolyte at a high voltage of 1.6 V. Furthermore, fitted Nyquist plots of the $Li_{0.5}Ni_{0.5}Ti_{1.5}Fe_{0.5}(PO_4)_3$/C electrode at different states of discharge and charge (Figure S5 and Table S3) confirm the increased cell resistance when the electrode was initially discharged to 1.85 V, confirming the formation of the SEI layer in this voltage range.

The obtained galvanostatic results were also confirmed by CV (Figure 4a inset), where the oxidation−reduction peaks of Fe^{2+}/Fe^{3+} appeared at 2.81 and 2.79 V, respectively. For the reduction of Ti^{4+} to Ti^{3+}, an intense peak was observed at the first discharge around 2.2 V, which was then shifted to ∼2.45 for the subsequent cycles. During the charge process, the oxidation peak of Ti^{3+} to Ti^{4+} appeared at around 2.6 V. Besides, an extra peak appeared at the end of the first reduction process (1.85 V), while it disappeared afterward, confirming the previously concluded result related to the formation of the SEI layer during the first discharge process at relatively high voltage (1.85 V).

Rate capability measurements revealed that the $Li_{0.5}Ni_{0.5}Ti_{1.5}Fe_{0.5}(PO_4)_3$/C material delivers an average specific capacity of about 110 mA h·g^{-1} at a current rate of 0.1 C. This capacity decreased slightly while cycling at the faster rate of 5 C by delivering a capacity of about 95 mA h·g^{-1} (Figure 4b). This rate-related performance is better than that obtained for $L_{1.5}Fe_{0.5}Ti_{1.5}(PO_4)_3$/C or other $LiTi_2(PO_4)_3$ material.[12,14]

The long-term cycling performance of the $Li_{0.5}Ni_{0.5}Ti_{1.5}Fe_{0.5}(PO_4)_3$/C material at the slow rate of 0.1 C was tested (Figure 4c). After 100 cycles, the $Li_{0.5}Ni_{0.5}Ti_{1.5}Fe_{0.5}(PO_4)_3$/C electrode material delivered a high reversible specific capacity of ∼115 mA h·g^{-1}, which corresponds to about 90% of its theoretical capacity. At the higher current rate of 5 C, about 91% of the initially obtained capacity (95 mA h·g^{-1}) was retained after 1000 cycles. Over the whole cycling process, the Coulomb efficiency of $Li_{0.5}Ni_{0.5}Ti_{1.5}Fe_{0.5}(PO_4)_3$/C was determined to be almost 100%, demonstrating the highly reversible lithium-ion insertion/disinsertion into and out of the $Li_{0.5}Ni_{0.5}Ti_{1.5}Fe_{0.5}(PO_4)_3$/C electrode material. These remarkable results can be directly related to the presence of Ni in the

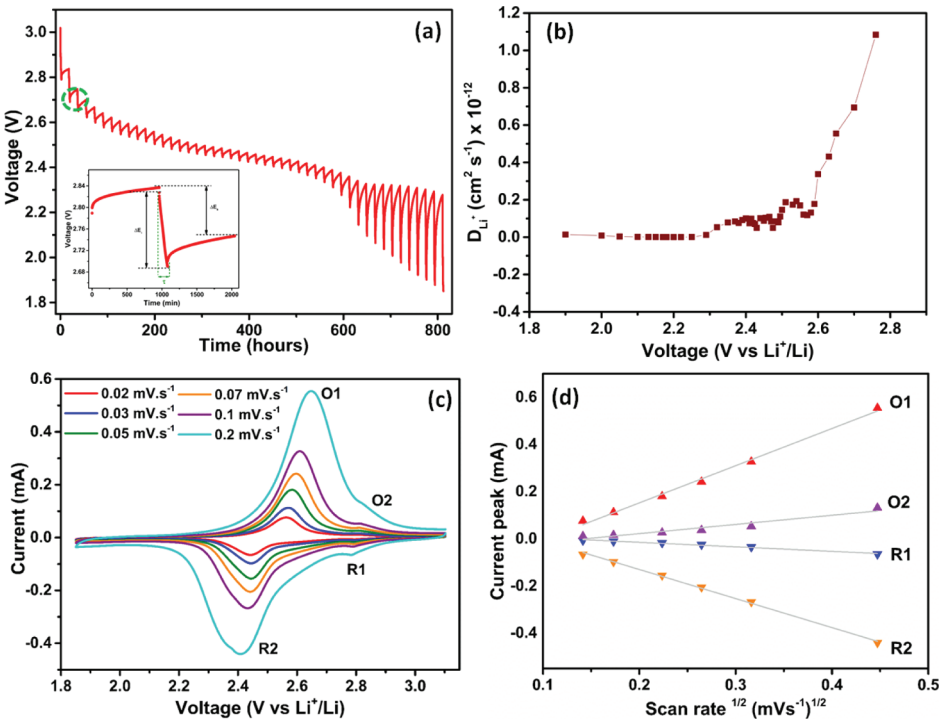

Figure 6. Electrochemical kinetics of the $Li_{0.5}Ni_{0.5}Ti_{1.5}Fe_{0.5}(PO_4)_3$/C material in the voltage range of 1.85−3.0 V vs Li^+/Li: (a) GITT curve during the first discharge−schema of the voltage response of the discharge pulse at ∼2.75 V vs Li^+/Li; (b) lithium ion diffusion coefficient calculated at different titrations; (c) CV at different scan rates; and (d) linear relation between the current peaks and square roots of scan rates.

lithium site of the NASICON structure. As it was mentioned before, the presence of nonactive divalent ions with an ionic radius of the same order as the one of lithium optimizes the lithium diffusion within the NASICON structure and facilitates the lithium intercalation into and out of the structure.[15,16] Another reason for this improved electrochemical performance of the $Li_{0.5}Ni_{0.5}Ti_{1.5}Fe_{0.5}(PO_4)_3$/C material compared to the previously studied LFTP@C[14] or other $LiTi_2(PO_4)_3$-based materials[12] can be related to the better electronic conductivity provided by nickel in the structure instead of lithium and the more stable structural network built with stronger Ni−O covalent bonds than Li−O bonds, leading to an improved long-term cycling stability.[16]

At the high current rate of 20 C, the material showed a very good reversibility with an initial discharge capacity of more than 80 mA h·g^{-1}. After 1000 cycles, the $Li_{0.5}Ni_{0.5}Ti_{1.5}Fe_{0.5}(PO_4)_3$/C electrode delivered ∼81% of this initial capacity.

The electrochemical behavior of the $Li_{0.5}Ni_{0.5}Ti_{1.5}Fe_{0.5}(PO_4)_3$/C material was also tested at lower voltages within the potential window 0.5−3.0 V versus Li^+/Li at a current rate of 0.1 C (Figure 5a). The first discharge profile was very different from the subsequent ones, with an excessive first discharge capacity of more than 620 mA h·g^{-1}. This capacity dropped to about 380 mA·h·g^{-1} after six cycles.

Similar to the electrochemical behavior obtained for the LFTP@C material,[14] the difference between the first discharge profile and the subsequent ones can be directly associated with the decomposition of the pristine structure while discharging to 0.5 V. Ex situ XRD analysis was performed at different states of discharge/charge between 0.5 and 3.0 V and confirmed the irreversible structural transformation that takes place once the electrode is discharged to 0.5 V versus Li^+/Li (Figure S4). Based on these results, the reaction mechanism in this voltage range can be considered similar to the one reported for $Mg_{0.5}Ti_2(PO_4)_3$.[26] Hence, after the first reaction that occurs in the first voltage range (1.85−3.0 V) allowing the insertion of two Li^+ ions into the structure, there should be one more remaining void in the $Li_{2.5}Ni_{0.5}Ti_{1.5}Fe_{0.5}(PO_4)_3$ structure for lithium insertion. The second Li^+-ion insertion reaction should take place at around 0.8 V (1.7 V lower than Ti^{3+}/Ti^{4+} redox potential versus Li^+/Li (2.48 V)) corresponding to the reduction of Ti^{3+} to Ti^{2+}. This would happen according to the following reaction

$$Li_{2.5}Ni_{0.5}Ti^{III}_{1.5}Fe^{II}_{0.5}(PO_4)_3 + 1.5Li^+ + 1.5e^- \rightarrow Li_4Ni_{0.5}Ti^{II}_{1.5}Fe^{II}_{0.5}(PO_4)_3$$

In addition to the Ti^{3+}/Ti^{2+} peak that should appear around 0.8 V, the CV curve shows a very strong reduction peak at 0.6 V. Meanwhile, all the M1 and M2 voids of the NASICON structure were occupied by Li^+ and Ni^{2+} with an extra 0.5 of Li^+. Further intercalation of Li^+ ions would thus lead to the decomposition of the pristine structure, according to the following reaction

$$Li_4Ni_{0.5}Ti^{II}_{1.5}Fe^{II}_{0.5}(PO_4)_3 + 5Li^+ + 5e^- \rightarrow 3Li_3PO_4 + 0.5Ni + 0.5Fe + 1.5Ti$$

Accordingly, during the first discharge, the complete Li^+ intercalation process into the $Li_{0.5}Ni_{0.5}Ti_{1.5}Fe_{0.5}(PO_4)_3$/C electrode involves 8.5 Li^+ ions that are inserted into the crystal structure, resulting in a theoretical capacity of 545.6 mA h·g^{-1}. The higher obtained experimental capacity (623.8 mA h·g^{-1}) can be attributed to the SEI phenomenon and its consumption of lithium ions, leading to the obtaining of the observed extra capacity. Furthermore, ex situ XRD analysis of the $Li_{0.5}Ni_{0.5}Ti_{1.5}Fe_{0.5}(PO_4)_3$/C electrodes at different states of

discharge and charge (Figure S4) confirmed the structural rearrangement, when the electrode is discharged below 0.6 V. Below this voltage, all the NASICON structure-related peaks disappeared. When the electrode is discharged to 0.5 V and then charged back to 3.0 V, the NASICON structure was not recovered, confirming the irreversibility of the conversion reaction that takes place at this low voltage.

The rate capability performance of the $Li_{0.5}Ni_{0.5}Ti_{1.5}Fe_{0.5}(PO_4)_3/C$ material at different current rates varying from 0.1 to 5 C was also tested at this potential window (Figure 5b). The material delivered its highest capacity at a slow rate of 0.1 C with an average of 380 mA $h{\cdot}g^{-1}$. At 5 C, the material delivered only a capacity of about 220 mA $h{\cdot}g^{-1}$. Unlike the acquired results at the smaller potential window of 1.85−3.0 V and because of the structural rearrangement taking place as demonstrated by the ex situ XRD, we have observed a very weak reversibility depending on the applied current at this potential range (0.5−3.0 V).

Electrochemical Kinetics. In order to evaluate the electrochemical kinetics of the $Li_{0.5}Ni_{0.5}Ti_{1.5}Fe_{0.5}(PO_4)_3/C$ material within the potential window of 1.85−3.0 V, for which a clear reversibility was observed, CV and GITT were employed to calculate the electrochemical lithium diffusion coefficient D^+_{Li}, in particular during the first discharge process. Figure 6a shows the GITT curve during first discharge at a very slow rate of 0.05 C (discharge for 2 h and then relaxation for 16 h). An example of a single discharge pulse at around 2.75 V is demonstrated in the inset of the same figure.

Moreover, the cell voltage during titration is considered to be linearly proportional to $\tau^{1/2}$ (Figure S6). Then, the chemical diffusion coefficient of the Li^+ ions can be calculated based on Fick's second law of diffusion through the simplified eq 1[27,28]

$$D_{Li^+} = \frac{4}{\pi\tau}\left(\frac{n_B V_m}{S}\right)^2\left(\frac{\Delta E_s}{\Delta E_\tau}\right)^2 \quad (1)$$

where τ is the duration of the current pulse (s); n_B is the number of moles (mol); V_m is the molar volume of the electrode ($cm^3\ mol^{-1}$); S is the electrode/electrolyte contact area (cm^2); ΔE_s is the steady-state voltage change due to the current pulse; and ΔE_τ is the voltage change during the constant current pulse. D^+_{Li} of the $Li_{0.5}Ni_{0.5}Ti_{1.5}Fe_{0.5}(PO_4)_3/C$ electrode was calculated at different voltages during discharge (Figure 6b), and the average D^+_{Li} value is ∼1.38×10^{-13} $cm^2\ s^{-1}$.

The CV technique was also used as a confirmative technique to determine the kinetics of Li^+ insertion and extraction in $Li_{0.5}Ni_{0.5}Ti_{1.5}Fe_{0.5}(PO_4)_3/C$. Figure 6c shows the redox reactions of $Ti^{4+}/T^{3+}$and Fe^{3+}/Fe^{2+}. The major redox reaction occurred at 2.4 and 2.65 V versus Li^+/Li at 0.2 mV s^{-1}, corresponding to Ti^{4+}/T^{3+} and the small redox peaks correspond to Fe^{3+}/Fe^{2+}. The potential difference between anodic and cathodic peaks became narrower while decreasing the scan rate.

Figure 6d shows that the cathodic (R1 and R2) and anodic (O1 and O2) current peaks are linearly dependent on the square root of the scan rate (R^2 of 0.98, 0.998, 0.995, and 0.933 for anodic and cathodic lines). Based on this relation, the Li^+ diffusion coefficient (D^+_{Li}) in the $Li_{0.5}Ni_{0.5}Ti_{1.5}Fe_{0.5}(PO_4)_3/C$ electrode is calculated using the Randles−Sevcik eq 2.[29]

$$I_p = (2.69 \times 10^5)n^{3/2}S{D_{Li^+}}^{1/2}Cv^{1/2} \quad (2)$$

where I_p is the current peak (in mA), n is the number of electrons, S is the surface area of the electrode (in $cm^2\ g^{-1}$), D is the diffusion coefficient (in $cm^2\ s^{-1}$), C is the concentration of Li^+ (mol cm^{-3}), and v is the scan rate (in mV s^{-1}).

The calculated D^+_{Li} for Li^+ insertion corresponding to Ti^{4+}/T^{3+} is 6.4×10^{-13} $cm^2\ s^{-1}$, which is in the order of magnitude of the averageD^+_{Li} obtained via the GITT, while that related to the extraction of Li^+ in Ti^{4+}/T^{3+} was higher, 1.05×10^{-12} $cm^2\ s^{-1}$ at 25 °C. These values are higher than the D^+_{Li} reported for $LiTi_2(PO_4)_3$ (1.55×10^{-14} and 1.31×10^{-14} $cm^2\ s^{-1}$ for the anodic and cathodic reactions, respectively) using the same CV technique[30] and are in quite the same order for the recently reported $Ni_{0.5}Ti_2(PO_4)_3$ delivering high electrochemical performances.[16]

On the other hand, the reduction current peak of Fe^{3+}/Fe^{2+} was about 10−15% of that of Ti^{4+}/T^{3+}, while the oxidation current peak of Fe^{3+}/Fe^{2+} was 15−24%, although the stoichiometric ratio of Fe is ca. 33% of that of Ti in the $Li_{0.5}Ni_{0.5}Ti_{1.5}Fe_{0.5}(PO_4)_3/C$ compound. These low redox current peaks of Fe^{3+}/Fe^{2+}reflected the low slope in Figure 6d, corresponding to $D^+_{Li} = 1.56 \times 10^{-14}$ and 6.38×10^{-14} $cm^2\ s^{-1}$ for Li^+ insertion and extraction, respectively. In both cases of Ti and Fe, the anodic current intensities were higher than the cathodic ones (Figure 6c), meaning that the kinetics of Li^+ extraction is faster than that of Li^+ insertion in the $Li_{0.5}Ni_{0.5}Ti_{1.5}Fe_{0.5}(PO_4)_3/C$ structure.

■ CONCLUSIONS

The $Li_{0.5}Ni_{0.5}Ti_{1.5}Fe_{0.5}(PO_4)_3$ NASICON material was synthetized via the sol−gel method and carbon coating of its particles was performed using sucrose. SEM and TEM images confirmed the nanosize and spherical shape of the primary particles of the studied material. When tested as an anode for lithium batteries, $Li_{0.5}Ni_{0.5}Ti_{1.5}Fe_{0.5}(PO_4)_3/C$ delivers a high reversible capacity of around 110 mA $h{\cdot}g^{-1}$ at a current rate of 0.1 C in the voltage range of 1.85−3.0 V versus Li^+/Li, with an excellent capacity retention of more than 96% after 100 cycles. At high C-rates such as 5 and 20 C, the $Li_{0.5}Ni_{0.5}Ti_{1.5}Fe_{0.5}(PO_4)_3/C$ electrodes deliver an initial capacity of 95 and 80 mA $h{\cdot}g^{-1}$ and remarkable capacity retention of 91 and 81% after 1000 cycles, respectively. When tested at lower voltages down to 0.5 V, the pristine NASICON structure of the material was deformed because of the excess of Li^+ insertion, confirmed with ex situ XRD patterns of $Li_{0.5}Ni_{0.5}Ti_{1.5}Fe_{0.5}(PO_4)_3/C$ at different states of charge.

■ ASSOCIATED CONTENT

Supporting Information

The Supporting Information is available free of charge at https://pubs.acs.org/doi/10.1021/acsami.0c00712.

Rietveld refinement resulting atomic positions and interatomic distances of $Li_{0.5}Ni_{0.5}Ti_{1.5}Fe_{0.5}(PO_4)_3$, XRD pattern of the carbon-coated $Li_{0.5}Ni_{0.5}Ti_{1.5}Fe_{0.5}(PO_4)_3/C$ material, statistical reparation of the obtained particles size using the ImageJ program, CV curves of the $Li_{0.5}Ni_{0.5}Ti_{1.5}Fe_{0.5}(PO_4)_3/C$ electrode in the voltage window 1.0−3.0 V, ex situ XRD patterns of the $Li_{0.5}Ni_{0.5}Ti_{1.5}Fe_{0.5}(PO_4)_3/C$ electrodes at different states of discharge/charge during the first cycle, EIS-related Nyquist plots of the $Li_{0.5}Ni_{0.5}Ti_{1.5}Fe_{0.5}(PO_4)_3/C$ electrode at different states of discharge/charge, and plot of

voltage versus $\tau^{1/2}$ and its linear fit during titration (GITT) (PDF)

AUTHOR INFORMATION

Corresponding Author

Ismael Saadoune − *IMED-Lab., Cadi Ayyad University (UCA), 40000 Marrakesh, Morocco; Mohammed VI Polytechnic University, 43150 Ben Guerir, Morocco;* orcid.org/0000-0003-1322-361X; Email: i.saadoune@uca.ma

Authors

Mohammed Srout − *IMED-Lab., Cadi Ayyad University (UCA), 40000 Marrakesh, Morocco; Department of Chemistry, University of Fribourg, 1700 Fribourg, Switzerland*

Nam Hee Kwon − *Department of Chemistry, University of Fribourg, 1700 Fribourg, Switzerland*

Hicham Ben Youcef − *Mohammed VI Polytechnic University, 43150 Ben Guerir, Morocco*

Nawal Semlal − *OCP, Innovation, 24000 El Jadida, Morocco*

Katharina M. Fromm − *Department of Chemistry, University of Fribourg, 1700 Fribourg, Switzerland;* orcid.org/0000-0002-1168-0123

Complete contact information is available at: https://pubs.acs.org/10.1021/acsami.0c00712

Notes

The authors declare no competing financial interest.

ACKNOWLEDGMENTS

This work was done with the financial support of the OCP group (Morocco) through the APPHOS Program (2017−2019). The authors further thank the Swiss Confederation for the excellence stipend for M.S., the University of Fribourg, the Swiss National Science Foundation, and the Adolphe Merkle Foundation (FriMat) for generous support.

REFERENCES

(1) Armand, M.; Tarascon, J.-M. Building Better Batteries. *Nature* **2008**, *451*, 652−657.

(2) Renewable Energy Directive. Renewables Get Mature. *Nat. Energy* **2017**, *2*, 17017.

(3) Scrosati, B.; Hassoun, J.; Sun, Y.-K. Lithium-Ion Batteries. A Look into the Future. *Energy Environ. Sci.* **2011**, *4*, 3287.

(4) Zhang, G.; Hou, S.; Zhang, H.; Zeng, W.; Yan, F.; Li, C. C.; Duan, H. High-Performance and Ultra-Stable Lithium-Ion Batteries Based on MOF-Derived ZnO@ZnO Quantum Dots/C Core-Shell Nanorod Arrays on a Carbon Cloth Anode. *Adv. Mater.* **2015**, *27*, 2400−2405.

(5) Goriparti, S.; Miele, E.; De Angelis, F.; Di Fabrizio, E.; Proietti Zaccaria, R.; Capiglia, C. Review on Recent Progress of Nano-structured Anode Materials for Li-Ion Batteries. *J. Power Sources* **2014**, *257*, 421−443.

(6) Chen, S.; Wu, C.; Shen, L.; Zhu, C.; Huang, Y.; Xi, K.; Maier, J.; Yu, Y. Challenges and Perspectives for NASICON-Type Electrode Materials for Advanced Sodium-Ion Batteries. *Adv. Mater.* **2017**, *29*, 1700431.

(7) Bruce, P. G.; Scrosati, B.; Tarascon, J.-M. Nanomaterials for Rechargeable Lithium Batteries. *Angew. Chem., Int. Ed.* **2008**, *47*, 2930−2946.

(8) Tao, D.; Wang, S.; Liu, Y.; Dai, Y.; Yu, J.; Lei, X. Lithium Vanadium Phosphate as Cathode Material for Lithium Ion Batteries. *Ionics* **2015**, *21*, 1201−1239.

(9) Wang, G. X.; Bradhurst, D. H.; Dou, S. X.; Liu, H. K. $LiTi_2(PO_4)_3$ with NASICON-Type Structure as Lithium-Storage Materials. *J. Power Sources* **2003**, *124*, 231−236.

(10) Jian, Z.; Hu, Y.-S.; Ji, X.; Chen, W. NASICON-Structured Materials for Energy Storage. *Adv. Mater.* **2017**, *29*, 1601925.

(11) Sun, D.; Xue, X.; Tang, Y.; Jing, Y.; Huang, B.; Ren, Y.; Yao, Y.; Wang, H.; Cao, G. High-Rate $LiTi_2(PO_4)_3$@N-C Composite via Bi-Nitrogen Sources Doping. *ACS Appl. Mater. Interfaces* **2015**, *7*, 28337−28345.

(12) Aravindan, V.; Ling, W. C.; Hartung, S.; Bucher, N.; Madhavi, S. Carbon-Coated $LiTi_2(PO_4)_3$: An Ideal Insertion Host for Lithium-Ion and Sodium-Ion Batteries. *Chem.—Asian J.* **2014**, *9*, 878−882.

(13) Kwon, N. H.; Conder, J.; Srout, M.; Fromm, K. M. Surface Modifications of Positive-Electrode Materials for Lithium Ion Batteries. *Chimia* **2019**, *73*, 880−893.

(14) Srout, M.; Lasri, K.; Dahbi, M.; Kara, A.; Tetard, L.; Saadoune, I. Understanding of the Li-Insertion Process in a Phosphate Based Electrode Material for Lithium Ion Batteries. *J. Power Sources* **2019**, *435*, 226803.

(15) Wu, Z.; Xie, Z.; Yoshida, A.; Wang, Z.; Hao, X.; Abudula, A.; Guan, G. Utmost Limits of Various Solid Electrolytes in All-Solid-State Lithium Batteries: A Critical Review. *Renew. Sustain. Energy Rev.* **2019**, *109*, 367−385.

(16) Srout, M.; Kwon, N. H.; Luo, W.; Züttel, A.; Fromm, K. M.; Saadoune, I. New $Ni_{0.5}Ti_2(PO_4)_3$@C NASICON-type Electrode Material with High Rate Capability Performance for Lithium-Ion Batteries: Synthesis and Electrochemical Properties. *ChemSusChem* **2019**, *12*, 4846.

(17) Rietveld, H. M. A Profile Refinement Method for Nuclear and Magnetic Structures. *J. Appl. Crystallogr.* **1969**, *2*, 65−71.

(18) Rodríguez-Carvajal, J. Recent Advances in Magnetic Structure Determination by Neutron Powder Diffraction. *Phys. B Condens. Matter* **1993**, *192*, 55−69.

(19) Aatiq, A.; Delmas, C.; El Jazouli, A. Structural and Electrochemical Study of $Li_{0.5}Mn_{0.5}Ti_{1.5}Cr_{0.5}(PO_4)_3$. *J. Solid State Chem.* **2001**, *158*, 169−174.

(20) Luo, J.-Y.; Chen, L.-J.; Zhao, Y.-J.; He, P.; Xia, Y.-Y. The Effect of Oxygen Vacancies on the Structure and Electrochemistry of $LiTi_2(PO_4)_3$ for Lithium-Ion Batteries: A Combined Experimental and Theoretical Study. *J. Power Sources* **2009**, *194*, 1075−1080.

(21) Aravindan, V.; Chuiling, W.; Reddy, M. V.; Rao, G. V. S.; Chowdari, B. V. R.; Madhavi, S. Carbon Coated Nano-$LiTi_2(PO_4)_3$ Electrodes for Non-Aqueous Hybrid Supercapacitors. *Phys. Chem. Chem. Phys.* **2012**, *14*, 5808.

(22) Wei, Z.; Pan, R.; Hou, Y.; Yang, Y.; Liu, Y. Graphene-Supported Pd Catalyst for Highly Selective Hydrogenation of Resorcinol to 1, 3-Cyclohexanedione through Giant π-Conjugate Interactions. *Sci. Rep.* **2015**, *5*, 15664.

(23) Shen, W.; Wang, C.; Xu, Q.; Liu, H.; Wang, Y. Nitrogen-Doping-Induced Defects of a Carbon Coating Layer Facilitate Na-Storage in Electrode Materials. *Adv. Energy Mater* **2014**, *5*, 1400982.

(24) Lu, C.-Z.; Fey, G. T.-K.; Kao, H.-M. Study of LiFePO4 Cathode Materials Coated with High Surface Area Carbon. *J. Power Sources* **2009**, *189*, 155−162.

(25) Vidal-Abarca, C.; Lavela, P.; Aragón, M. J.; Plylahan, N.; Tirado, J. L. The Influence of Iron Substitution on the Electrochemical Properties of $Li_{1+x}Ti_{2-x}Fe_x(PO_4)_3$/C Composites as Electrodes for Lithium Batteries. *J. Mater. Chem.* **2012**, *22*, 21602.

(26) Zhao, Y.; Wei, Z.; Pang, Q.; Wei, Y.; Cai, Y.; Fu, Q.; Du, F.; Sarapulova, A.; Ehrenberg, H.; Liu, B.; Chen, G. NASICON-Type $Mg_{0.5}Ti_2(PO_4)_3$ Negative Electrode Material Exhibits Different Electrochemical Energy Storage Mechanisms in Na-Ion and Li-Ion Batteries. *ACS Appl. Mater. Interfaces* **2017**, *9*, 4709.

(27) Deiss, E. Spurious Chemical Diffusion Coefficients of Li^+ in Electrode Materials Evaluated with GITT. *Electrochim. Acta* **2005**, *50*, 2927−2932.

(28) Weppner, W. Determination of the Kinetic Parameters of Mixed-Conducting Electrodes and Application to the System Li[Sub 3]Sb. *J. Electrochem. Soc.* **1977**, *124*, 1569.

(29) Bard, A. J.; Faulkner, L. R. *Electrochemical Methods Fundamentals and Applications*, 2nd ed.; Harris, D., Swain, E., Aiello, E., Eds.; John Wiley & Sons, Inc., 2001.

(30) Roh, H.-K.; Kim, H.-K.; Roh, K. C.; Kim, K.-B. $LiTi_2(PO_4)_3$/Reduced Graphene Oxide Nanocomposite with Enhanced Electrochemical Performance for Lithium-Ion Batteries. *RSC Adv.* **2014**, *4*, 31672−31677.